Meteorol Atmos Phys 82, 259–270 (2003)
DOI 10.1007/s00703-001-0589-4

Meteorology and Atmospheric Physics
Printed in Austria

Institute for Applied Mathematics, University of Freiburg, Germany

Finite volume method on unstructured grids in 3D with applications to the simulation of gravity waves

L. Klassen, D. Kröner, and **Ph. Schott**

With 8 Figures

Received April 20, 2001; revised September 10, 2001
Published online: November 21, 2002

Summary

A code for the simulation of atmospheric flows in 3D is presented. The underlying mathematical model is fully compressible, it takes gravity into account but Coriolis forces, turbulence and viscosity are neglected. The general numerical code consists of a finite volume discretization on unstructured hexahedral grids in 3D. The code is presently being investigated on applications to the calculation of atmospheric gravity waves on a mesh which has a structured type and is locally refined near the orography. We develop two schemes, the main difference between them lies in the different discretizations for the mass fluxes. We show that both schemes resolve typical structures of gravity waves in potential flow, linear hydrostatic motion and nonlinear non-hydrostatic regime. We compare advantages and disadvantages of the developed schemes.

1. Introduction

In this paper we will apply an upwind finite volume scheme for the problem of gravity waves in atmospheric flow. Four different test cases will be considered:

(1) Static atmosphere or atmosphere moving with a constant velocity;
(2) Potential flow;
(3) Linear hydrostatic regime;
(4) Nonlinear non-hydrostatic regime.

As the mathematical model for these test problems, we consider the nonlinear system of the Euler equations of gas dynamics, i.e. the conservation of mass, momentum and energy for the inviscid, compressible flow. In addition we consider suitable boundary and initial conditions. These problems have been treated in several papers (see Bonaventura, 2000; Pinty et al, 1995 and the literature cited there).

We use grids which approximate the orography by piecewise linear functions, such as shown in Fig. 1. The piecewise linear representation provides a better approximation to the orography in comparison with the approximation by constant functions used in case of finite difference discretization (see Adcroft et al, 1997). In our case we prefer a grid consisting of hexahedrons, since in the viscous case (which will not be considered in this paper, but for later applications) the boundary layer at the lower boundary can be resolved much better by hexahedrons than by tetrahedrons or prisms. We define two new schemes in conservation form, which are special versions of the advection upstream splitting method (AUSM) by Liou (1993). The AUSM was developed and tested for weightless compressible fluids. Our versions are developed specifically for the case where the gravity influence on the fluid dynamics is important. We have to use upwind- or upstream-schemes (i.e., schemes which use the information only from the upwind

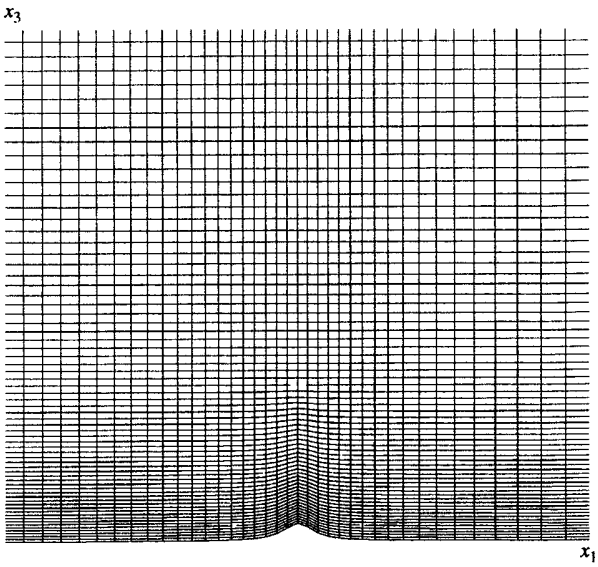

Fig. 1. Vertical section of the computational grid in a potential flow case

direction domain) since central schemes applied to conservation laws are known to be unstable (see Kröner, 1996, § 2.4). Note that for test problems performed in the case without gravity, the AUSM has turned out to be the most efficient and most accurate one compared to other numerical schemes for Euler equations (Wada and Liou, 1995). In particular, for shear flows in compressible viscose fluid it also gives excellent results (see Egelja et al, 1998). For the time discretization we use a simple explicit Euler step. Although we know that for the tests presented in this paper we expect stationary solutions and that in this case an implicit method is much more efficient, we decided to use an explicit one since we want to use this code also for non-stationary cases with steep gradients and fronts. It is known (see Kröner, 1996, p. 85) that in such cases, in particular for parallelization, the explicit method is much more efficient and produces less numerical diffusion than the implicit one. In Küther (2001) it was shown that an implicit scheme with arbitrary large time steps and Newton method for solving the non-linear discrete system does not have any advantage concerning numerical costs compared to explicit finite volume schemes with CFL restrictions. This is pointed out in more details in Küther (2001) for getting numerical approximations for discontinuous solutions of nonlinear conservation laws.

On the basis of the results of this paper we can use our tools concerning higher oder discretization of the convective terms, automatic grid refinement and parallelization including dynamic load balancing, in order to develop an efficient numerical code for flow simulations at mesoscale. We are going to show this in a forthcoming paper.

2. Mathematical model

2.1 Equations

The underlying mathematical model describes a flow which is compressible, time-dependent, three-dimensional, inviscid and adiabatic. It consists of the balance equations for mass, momentum and energy

$$\partial_t \rho + \nabla \cdot (\rho \mathbf{v}) = 0, \tag{1}$$

$$\partial_t(\rho v_{x_i}) + \nabla \cdot (\rho v_{x_i}\mathbf{v} + p\vec{\delta_i}) = \rho g_{x_i} \quad (i = 1,2,3), \tag{2}$$

$$\partial_t e + \nabla \cdot ((e+p)\mathbf{v}) = \rho \mathbf{v}\mathbf{g}, \tag{3}$$

as well as an equation of state for ideal gas

$$p = (\gamma - 1)\left(e - \frac{\rho \mathbf{v}^2}{2}\right). \tag{4}$$

Equations (1)–(4) present a conservative form of the Euler equations with source terms. They are considered in a Cartesian coordinate system (x_1, x_2, x_3) and have to be solved in the computational domain

$$\Omega = \{(x_1,x_2,x_3) \in \mathbb{R}^3 | x_1^{\min} \le x_1 \le x_1^{\max}, \; x_2^{\min} \le x_2 \le x_2^{\max}, f(x_1,x_2) \le x_3 \le x_3^{\max}\}, \tag{5}$$

where f describes the orography profile. The following notations are used: $\partial_t = \partial/\partial t$, $\nabla = (\partial/\partial x_1, \partial/\partial x_2, \partial/\partial x_3)$, $\vec{\delta_i} = (\delta_{i1}, \delta_{i2}, \delta_{i3})^T$, where δ_{ij} denotes the Kronecker-symbol. Vector $\mathbf{g}$ with components $g_{x_1} = 0$, $g_{x_2} = 0$, $g_{x_3} = -g$ is the gravity acceleration vector, $\mathbf{v} := (v_{x_1}, v_{x_2}, v_{x_3})^T$ is the velocity vector, and $\gamma = c_p/c_V$ is the adiabatic exponent. The constant parameters c_p and c_V are the specific heat capacities at constant pressure and constant volume respectively. With conservative variables ρ (density), $\rho\mathbf{v}$ (momentum vector), e (sum of the internal and kinetic energy), and p (pressure) there are six unknowns in the system (1)–(4).

For ideal gases there exists (see Pichler, 1997) a linear dependence between the internal energy per unit mass and the temperature T

$$e/\rho - \mathbf{v}^2/2 = c_V T. \tag{6}$$

Equation (6) is used in the model (1)–(4) for the calculation of the temperature distribution in the atmosphere. Another frequently used variable is the potential temperature θ defined as follows:

$$\theta = T(p_0/p)^{R/c_p}.$$

Here p_0 is the constant pressure which will be defined below, $R = c_V(\gamma - 1)$ is the gas constant.

2.2 Boundary conditions

The following boundary conditions are imposed. At the lower boundary $x_3 = f(x_1, x_2)$, the normal component of the velocity is zero

$$(\rho\mathbf{v}) \cdot \mathbf{n} = 0. \tag{7}$$

At the inflow ($x_1 = x_1^{\min}$) and at the upper boundary ($x_3 = x_3^{\max}$) the Dirichlet conditions

$$\rho = \rho^0, \quad \rho\mathbf{v} = \rho^0 (U, 0, 0)^T \tag{8}$$

are used with ρ^0 defined as in (10), (12). At the outflow ($x_1 = x_1^{\max}$) and on the "back" ($x_2 = x_2^{\max}$) and "front" ($x_2 = x_2^{\min}$) boundaries, the Neumann conditions are imposed:

$$\frac{\partial(\rho\mathbf{v} \cdot \mathbf{n})}{\partial n} = 0. \tag{9}$$

In (8), U is a given constant inflow velocity.

2.3 Initial data

In order to describe initial data, it is suitable to present first two stationary solutions of the problem (1)–(5) with boundary conditions (7)–(9). If $U = 0$ in (8), the problem has a stationary solution given by

$$\rho^0 = \rho_0 e^{-x_3/H_0}, \quad p^0 = p_0 e^{-x_3/H_0},$$
$$e^0 = p^0/(\gamma - 1), \quad x_3 > f(x_1, x_2), \tag{10}$$

$$(\rho\mathbf{v})^0 = (0, 0, 0)^T. \tag{11}$$

This solution, with $H_0 := p_0/(\rho_0 g)$, determines the distribution of the density, pressure and energy in a motionless isothermal model atmosphere with the temperature $T^0 = p_0/(\rho_0 R)$. The parameters p_0, ρ_0 are respectively the constant pressure and density at the lower boundary of the motionless isothermal atmosphere without orography, i.e. with $f(x_1, x_2) \equiv 0$.

If $f(x_1, x_2) \equiv 0$, in (5), then for all $U \neq 0$ there exists a stationary solution of the problem (1)–(5), (7)–(9) determined by

$$\rho^0 = \rho_0 e^{-x_3/H_0}, \quad p^0 = p_0 e^{-x_3/H_0},$$
$$e^0 = p^0/(\gamma - 1) + \rho^0 U^2/2, \tag{12}$$

$$(\rho\mathbf{v})^0 = \rho^0 (U, 0, 0)^T. \tag{13}$$

For all test problems in this paper we consider (1)–(4) in Ω with boundary conditions (7)–(9) and initial conditions given in domain Ω by (12), (13). For the four test cases we use different domains (5) and different inflow velocities U in boundary conditions (8) and initial data (13).

3. Numerical method

3.1 Discretization by finite volume scheme

For the discretization of the system (1)–(5), with boundary conditions (7)–(9) and initial data (12), (13), we use equation

$$\partial_t(\rho v_{x_i}) + \nabla \cdot (\rho v_{x_i}\mathbf{v} + (p - p^0)\vec{\delta}_i)$$
$$= (\rho - \rho^0) g_{x_i} \quad (i = 1, 2, 3), \tag{14}$$

instead of (2), where p^0 and ρ^0 are given by (10). Equation (14) is equivalent to (2).

The discretization consists of an explicit time dependent upwind finite volume scheme (see Kröner, 1997)

$$\mathbf{q}_i^{n+1} = \mathbf{q}_i^n - \frac{(\Delta t)_n}{|T_i|} \sum_{j \in \mathbb{N}(i)} \mathbf{G}_{ij}(\mathbf{q}_i^n, \mathbf{q}_j^n) + (\Delta t)_n \, \mathbf{r}_i^n \tag{15}$$

on an irregular hexahedral 3D mesh constructed by Schott (2001) (see, e.g., Fig. 1). Here $T_i, i \in \mathbb{N}$ denote the cells of the grid, $\mathbf{q}_i^{n+1}$ is the element-wise constant approximation of the exact solution $\mathbf{q} = (\rho, \rho v_{x_1}, \rho v_{x_2}, \rho v_{x_3}, e)^T$ in the cell T_i with its volume $|T_i|$ at the time $\sum_{i=1}^{n+1} (\Delta t)_i$. The indices of the neighbouring cells of T_i are denoted by $N(i)$. The right side is discretized by $\mathbf{r}_i^n = (0, 0, 0, (\rho_i^n - \rho_i^0)g, -g\rho_i(v_{x_3})_i)^T$.

3.2 Numerical flux

Now we present the definition for the flux $\mathbf{G}_{ij}$ between the cells i and j. The flux $\mathbf{G}_{ij}$ has to be

calculated perpendicular to the face S_{ij} of the cell T_j. We denote first through v the projection of the velocity vector $\mathbf{v}$ onto the normal $\mathbf{n}$ of the face S_{ij} and through u, w, and h – respectively the tangential projections of $\mathbf{v}$ on S_{ij} and the enthalpy of the gas per unit mass, $h := (e+p)/\rho$. Then we define the flux as follows:

$$\mathbf{G}_{ij}(\mathbf{q}_i, \mathbf{q}_j) := \frac{1}{2}\begin{pmatrix} 2(\rho v)_{ij} \\ 2(\rho v^2)_{ij} + 2(p-p^0)_{ij} \\ (\rho v)_{ij}(u_i+u_j) - |(\rho v)_{ij}|(u_j-u_i) \\ (\rho v)_{ij}(w_i+w_j) - |(\rho v)_{ij}|(w_j-w_i) \\ (\rho v)_{ij}(h_i+h_j) - |(\rho v)_{ij}|(h_j-h_i) \end{pmatrix}. \tag{16}$$

For the flux of the non-hydrostatic pressure $(p-p^0)_{ij}$ we propose

$$(p-p^0)_{ij} := p_i^+ + p_j^- - (p_i^0 + p_j^0)/2, \tag{17}$$

where p_i^0, p_j^0 are the values of hydrostatic pressure p^0 in the gravity centres of cells i, j, the pressures p_i^+, p_j^- are defined as in the AUSM scheme (see Liou, 1993):

$$p_i^+ := \begin{cases} p_i \frac{(v_i+c_m)^2}{4c_m^2}\left(2 - \frac{v_i}{c_m}\right), & \text{if } |v_i| \le c_m \\ p_i \frac{v_i+|v_i|}{2v_i} & \text{otherwise,} \end{cases} \tag{18}$$

$$p_j^- := \begin{cases} p_j \frac{(v_j-c_m)^2}{4c_m^2}\left(2 + \frac{v_j}{c_m}\right) & \text{if } |v_j| \le c_m \\ p_j \frac{v_j-|v_j|}{2v_j} & \text{otherwise,} \end{cases} \tag{19}$$

$c_m := \max(\sqrt{(\gamma p_i/\rho_i)}, \sqrt{(\gamma p_j/\rho_j)})$. In the latter formula i, j are given by (17).

To complete the definition of the flux $\mathbf{G}_{ij}$, it remains to define the mass flux $(\rho v)_{ij}$ and the normal momentum flux $(\rho v^2)_{ij}$. Now in Sects. 3.3 and 3.4, we construct two schemes with the above form of $\mathbf{G}_{ij}$, but different definitions for $(\rho v)_{ij}$ and $(\rho v^2)_{ij}$.

3.3 The scheme with the AUSM, U-splitting mass flux

In the first scheme, the mass flux in (16) is defined as follows:

$$(\rho v)_{ij} := \frac{1}{2}(v_{ij}(\rho_i+\rho_j) - |v_{ij}|(\rho_j-\rho_i)) \tag{20}$$

with

$$v_{ij} := v_i^+ + v_j^-, \tag{21}$$

and

$$v_i^+ := \begin{cases} \frac{(v_i+c_m)^2}{4c_m} & \text{if } |v_i| \le c_m \\ \frac{v_i+|v_i|}{2} & \text{otherwise,} \end{cases} \tag{22}$$

and

$$v_j^- := \begin{cases} -\frac{(v_j-c_m)^2}{4c_m} & \text{if } |v_j| \le c_m \\ \frac{v_j-|v_j|}{2} & \text{otherwise.} \end{cases} \tag{23}$$

The mass flux (20) has the form of the advection upstream splitting method (AUSM), U-splitting by Liou (1993). The normal momentum flux in (16) is determined by

$$(\rho v^2)_{ij} := \frac{1}{2}[(\rho v)_{ij}(v_i+v_j) - |(\rho v)_{ij}|(v_j-v_i)]. \tag{24}$$

Formulae (15)–(24) define the numerical scheme to which we shall refer as to the scheme with the AUSM, U-splitting mass flux.

Let us make some comments on the scheme (15)–(24). One can show that the convection and acoustic propagation are treated separately in this scheme. Really, with the help of (20), (24), the flux (16) can be written as a sum of the convective and pressure fluxes, $\mathbf{G}_{ij}^c$ and $\mathbf{G}_{ij}^p$, as follows:

$$\mathbf{G}_{ij}(\mathbf{q}_i, \mathbf{q}_j) = \mathbf{G}_{ij}^{(c)}(\mathbf{q}_i, \mathbf{q}_j) + \mathbf{G}_{ij}^{(p)}(\mathbf{q}_i, \mathbf{q}_j)$$

$$= v_{ij}\begin{cases} \Phi_i & \text{if } v_{ij} \ge 0 \\ \Phi_j & \text{otherwise,} \end{cases} + \begin{pmatrix} 0 \\ 2(p-p^0)_{ij} \\ 0 \\ 0 \\ 0 \end{pmatrix},$$

where $\Phi_{i/j} = (\rho, \rho v, \rho w, \rho u, \rho h)_{i/j}^T$, the pressure-difference $(p-p^0)_{ij}$ and velocity v_{ij} at the cell interface are defined by (17) and (21) respectively. We see that v_{ij} can be treated as the advection velocity, i.e. as the velocity at which the convective quantities, which are the components of the vector $\Phi_{i/j}$, are transfered. The convective flux $\mathbf{G}_{ij}^{(c)}(\mathbf{q}_i, \mathbf{q}_j)$ depends on the sign of the advection velocity v_{ij} in such a way that the advective quantities at the cell interface are determined with the help of the upwind extrapolation. The split functions (18), (19), (22) and (23) are defined by using the characteristic speeds of the acoustic waves traveling towards the face S_{ij} from the adjacent cells T_i and T_j. We use here these definitions because, in the case without

gravity, they have been successfully tested by Liou (1993), Liou and Wada (1993). The second-order polynomials $(v_i + c_m)^2$ and $(v_j - c_m)^2$ are used in the split functions for the subsonic region. This is made because it yields the functions $p_i^+(v_i), v_i^+(v_i)$ and $p_j^-(v_j), v_j^-(v_j)$ differentiable at $|v_{i/j}| = c_m$.

We show now that the scheme (15)–(24) reproduces the static isothermal atmosphere (10), (11) at every time step n under appropriate discretization of the boundary conditions (see Sect. 3.5 below). Really, with $v_i = v_j = 0$, from (22), (23) it follows that $v_i^+ = -v_i^- = c_0/4$ with $c_0 := \sqrt{(\gamma p_0/\rho_0)}$. Thus we have $v_{ij} = 0$ in (21). Hence the mass flux (20) is equal to zero. From (24) it follows that $(\rho v^2)_{ij} = 0$. From (18), (19) we obtain $p_i^+ = p_i^0/2, p_j^- = p_j^0/2$. Therefore, in (17), the pressure difference $(p - p^0)_{ij}$ is equal to zero. Consequently, all components of the flux vector (16) are zero. Since, for the motionless isothermal atmosphere (10), we have $\mathbf{r}_i^n = 0$ in Eq. (15), it follows that $\mathbf{q}_i^{n+1} = \mathbf{q}_i^n$ for every time step n.

Note that the study by Wada and Liou (1997) shows the mass flux (20) to be not appropriate for construction of schemes for problems with strong discontinuities, because the use of the discretization (20) leads to overshoots at shock waves. We propose, therefore, the scheme (15)–(24) for simulations of compressible gravity-dependent flows without strong discontinuities.

Notice, that for the normal momentum flux $(\rho v^2)_{ij}$ we have tested also a splitting defined as follows:

$$(\rho v^2)_{ij} := v_i^+(\rho v)_i + v_j^-(\rho v)_j, \tag{25}$$

as well as a linear combination of (24) and (25), constructed analogously to that one as described by Wada and Liou (1997) in the development of their AUSMDV scheme. In the test problems, we did not find any advantage of the schemes which include discretization (25).

3.4 The scheme with the density splitting

In the second scheme we present the mass flux in (16) as a sum of two fluxes

$$(\rho v)_{ij} := (\rho^0 v)_{ij} + [(\rho - \rho^0)v]_{ij}. \tag{26}$$

For the mass flux $(\rho^0 v)_{ij}$ with the hydrostatic density, we use the AUSM, U-splitting form

$$(\rho^0 v)_{ij} := \frac{1}{2}(v_{ij}(\rho_i^0 + \rho_j^0) - |v_{ij}|(\rho_j^0 - \rho_i^0)), \tag{27}$$

where v_{ij} is defined as in (21). The mass flux $[(\rho - \rho^0)v]_{ij}$ is defined as follows:

$$[(\rho - \rho^0)v]_{ij} := v_i^+(\rho_i - \rho_i^0) + v_j^-(\rho_j - \rho_j^0). \tag{28}$$

In (28), the velocities v_i^+, v_i^- are defined by (22), (23), respectively. Discretization (28) is analogous to that one used by Van Leer (1991) for the mass flux in the case without gravity field. The difference between the discretization (28) and that one by Van Leer is that we discretize only the part of the mass flux, which corresponds to the deviation $(\rho - \rho^0)$ of the density ρ from the hydrostatic density ρ^0.

Notice that the use of the Van Leer's splitting

$$(\rho v)_{ij} := v_i^+\rho_i + v_j^-\rho_j \tag{29}$$

for the total mass flux $(\rho v)_{ij}$ in (16) would lead for the static isothermal atmosphere (10), (11) to $(\rho v)_{ij} = (\rho_i^0 - \rho_j^0)c_0/4 \neq 0$, and, as a consequence, it would lead to an excessive numerical dissipation confirmed by our numerical simulations.

For the definition of the normal momentum flux $(\rho v^2)_{ij}$ in (16) we used the idea by Wada and Liou (1997) to construct a linear combination of two different splittings. For the normal momentum flux $(\rho v^2)_{ij}$, we construct a sum

$$(\rho v^2)_{ij} = (1+s)[(\rho - \rho^0)v^2]_V + (1-s)[(\rho - \rho^0)v^2]_D + 2(\rho^0 v^2)_{ij} \tag{30}$$

with

$$(\rho^0 v^2)_{ij} := \frac{1}{2}[(\rho^0 v)_{ij}(v_i + v_j) - |(\rho^0 v)_{ij}|(v_i - v_j)], \tag{31}$$

$$[(\rho - \rho^0)v^2]_V := v_i^+[(\rho - \rho^0)v]_i + v_j^-[(\rho - \rho^0)v]_j, \tag{32}$$

$$[(\rho - \rho^0)v^2]_D := \frac{1}{2}[[(\rho - \rho^0)v]_{ij}(v_i + v_j) - |[(\rho - \rho^0)v]_{ij}|(v_i - v_j)]], \tag{33}$$

v_i^+, v_j^- as in (22), (23), $(\rho^0 v)_{ij}$, $[(\rho - \rho^0)v]_{ij}$ defined by (27), (28), and

$$s := \min\{1, K(p_i - p_j)/\min(p_i^0, p_j^0)\}.$$

In the latter formula, K is a constant and for the test problems presented in this paper the value $K = 10$ has been used.

We use the subscripts V, D in (32), (33) in order to stress that the splitting of (32), (33) is similar to the AUSMV and AUSMD, respectively, as introduced by Wada and Liou (1997) but the definitions for v_i^+, v_j^- in (22), (23) and, thus also for v_{ij} in (21), differ from the corresponding definitions in Wada and Liou (1997).

Note that Wada and Liou (1997) have shown the use of two different splittings (AUSMV, AUSMD) in the normal momentum discretization together with the Van Leer's splitting (29) in the mass flux discretization to be very effective for a good resolution of shock waves in weightless gases. It makes, therefore, reasonable to assume the scheme (15)–(19), (21)–(23), (26)–(28), (30)–(33) to be applicable also to problems with strong discontinuities for compressible fluids in gravity field. We shall call the discretization (15)–(19), (21)–(23), (26)–(28), (30)–(33) the density splitting scheme. The density splitting scheme reproduces the motionless isothermal atmosphere. This can be shown similarly as in the case of the AUSM, U-splitting mass flux.

3.5 Discretization of the boundary conditions

To implement the boundary conditions we construct the ghosts cells for all boundary hexahedrons. On every boundary face, the adjacent hexahedron is reflected into the outer domain. In the ghost cells which touch the inflow and the upper boundary, the Dirichlet conditions are given. At the outflow boundaries, the Neumann conditions are implemented by means of constant extrapolation of the corresponding values from the first inner hexahedrons. Then, all six required fluxes in the inner boundary cells can be calculated. For calculations of the numerical fluxes in boundary cells at the lower boundary, the values in ghost cells are given as follows. For the numerical scheme with the AUSM, U-splitting mass flux they are given by

$$\rho_{gi} = \rho_i, \quad v_{gi} = -v_i, \quad e_{gi} = e_i - 2\rho_i v_i^2,$$
$$p_{gi} = p_{gi}^0 + p_i - p_i^0. \tag{34}$$

For the scheme with the density splitting, v_{gi} and p_{gi} are given as in (34), while ρ_{gi} and e_{gi} are determined by

$$\rho_{gi} = \rho_{gi}^0 + \rho_i - \rho_i^0, \quad e_{gi} = e_i - 2\rho_i v_i^2 + (\rho_{gi} - \rho_i)[p_i/((\gamma - 1)\rho_i) - v_i^2/2]. \tag{35}$$

The index gi denotes the ghost cell constructed by the symmetrical reflection of the boundary element T_i. We denote through ρ_{gi}^0, p_{gi}^0 the values of the density and pressure in the gravity center of the ghost cell gi, which are determined by (12). The choice of ρ_{gi} in (34), (35) ensures the absence of mass transfer across the mountain surface. The choice for p_{gi} in (34) guarantees no net transfer for the normal momentum across the mountain surface in the reference state (10), (11). Note that Pinty et al (1995), and Bonaventura (2000) consider the Neumann condition $\partial_n \theta = 0$ for the potential temperature θ as the numerical boundary condition at the lower boundary. Our choice for e_{gi} corresponds to the numerical boundary condition $\partial_n T = 0$ for the temperature T given by (6). If we extend our model to the viscous case, then we can use the condition $\partial_n T = 0$ as the physical boundary condition. Our numerical solutions approximate the corresponding solutions of the compressible Navier–Stokes equations at small coefficients of the viscosity and the heat diffusion in the idealized case of thermally insulated mountain (see, e.g., p. 443 in Oliger and Sundström, 1978).

Near the upper, inflow and outflow boundaries, we have to introduce dissipative layers (see Klemp and Lilly, 1978). Such a modification of the boundary conditions is necessary in order to avoid the reflection of outgoing gravity waves. We do this by using the known sponge layers technique proposed by Pinty et al (1995).

4. Test problems

We consider the following test problems: static atmosphere or atmosphere moving with a constant velocity, potential flow, linear hydrostatic regime, and nonlinear non-hydrostatic regime. In the first case we consider the isothermal atmosphere. In the latter three cases we restrict the consideration to the model atmosphere which is isothermal in the motionless state.

If the reference state is the isothermal atmosphere moving with a constant velocity, then the Euler equations linearized around this state admit stationary solutions describing 2D waves over a long symmetric mountain with a very small characteristic height (linear hydrostatic waves, see Pichler, 1997). These waves have a periodic structure in the vertical direction, and they quickly decay in the horizontal direction with

growing distance from the mountain symmetry-plane. Other possible regimes are non-linear non-hydrostatic motion and potential flow. They occur over smaller scale mountains. The nonlinear non-hydrostatic motion (lee waves) occurs under considerably small overflow velocities. The classical lee waves are the quasi-periodic waves extending downstream from a mountain. The potential flow is the mountain overflow without formation of lee waves. The flow becomes potential, if the characteristic overflow time is much smaller than the period of gravity oscillations equal to $2\pi/N$ with

$$N := g/\sqrt{c_p T^0} \tag{36}$$

the Brunt-Vaisala frequency. Such flow occurs under large overflow velocities. The described wave regimes have been used in recent works by Pinty (1995), Bonaventura (2000) in order to test the numerical codes for atmospheric flows.

For all tests, the physical parameters have the same values: $c_p = 1004\,\mathrm{J/(kg\,K)}$, $c_V = 717\,\mathrm{J/(kg\,K)}$, $g = 9.81\,\mathrm{m/sec^2}$, $\rho_0 = 1.225\,\mathrm{kg/m^3}$, $p_0 = 101325\,\mathrm{Pa}$. Equations (1)–(9) are used in dimensionless form, and all results below will be also presented in the dimensionless form. For dimensionless variables we shall keep the same notations as for the corresponding dimensional ones. To transfer the results into dimensional form, the following characteristic scales have to be used:

Variable	Scale	Value in MS
density	ρ_0	$1.225\,\mathrm{kg/m^3}$
velocity	$\sqrt{p_0/\rho_0}$	287.60 m/sec
pressure	p_0	101325 Pa
length	H	20000 m
time	$H/\sqrt{p_0/\rho_0}$	65.54 sec
temperature	$p_0/(\rho_0 R)$	288.15 K

We performed simulations with Courant numbers smaller or equal to 0.5.

4.1 Static atmosphere or atmosphere moving with a constant velocity

In order to validate the numerical code we have considered in this section the following test problems:

Test problem 1: Static atmosphere without orography. We consider (1)–(5) with boundary conditions (7)–(9), $f(x_1, x_2) \equiv 0$ and initial data given by (10), (11). The exact solution $\mathbf{q}_1^0$ is given by (10), (11).

Test problem 2: Atmosphere without orography, moving with a constant velocity. We consider (1)–(5) with boundary conditions (7)–(9), $f(x_1, x_2) \equiv 0$ and initial data given by (12), (13). The exact solution $\mathbf{q}_2^0$ is given by (12), (13).

Test problem 3: Static atmosphere with orography. The same as the test problem 1, but $f(x_1, x_2)$ is given by the Agnesi profile

$$f(x_1, x_2) := \frac{h_0}{1 + (x_1/a)^2}, \tag{37}$$

with the height h_0 and the half-width a. The exact solution is given by (10), (11).

Note that, in the presence of the orography (i.e., for $f \neq 0$), we cannot expect the solution (12), (13) with $U \neq 0$, since, in the problem under consideration, these data will not satisfy the boundary condition (7).

For all test problems we apply the AUSM, U-splitting mass flux and the scheme with the density splitting, defined by the formulas (15)–(24) and (15)–(19), (21)–(23), (26)–(28), (30)–(33) correspondingly.

In the first two problems, the solutions $\mathbf{q}_1^0$ and $\mathbf{q}_2^0$ describe respectively the state of the motionless isothermal atmosphere and of the isothermal atmosphere moving with a constant velocity U along the horizontal plane. We compute the numerical solutions $\mathbf{q}_1^{\mathrm{num}}$ and $\mathbf{q}_2^{\mathrm{num}}$ in the domain

$$\Omega = \{(x_1, x_2, x_3) \in \mathbb{R}^3 \mid -5 \le x_1 \le 5, \quad 0 \le x_2 \le 0.2,\ 0 \le x_3 \le 1\} \tag{38}$$

on grids with cell diameter $l \approx 0.25$ until the time $t = 5000$ at which we calculate L^1 errors. We compute the solution $\mathbf{q}_2^0$ with $U = 0.111$ in the boundary condition (9) and initial data (13). For both numerical schemes, the AUSM, U-splitting mass flux and the scheme with the density splitting, the L^1 errors $\|q_{1,k}^0 - q_{1,k}^{\mathrm{num}}\|_L^1$ and $\|q_{2,k}^0 - q_{2,k}^{\mathrm{num}}\|_L^1$ for each component k $(k = 1, \ldots, 5)$ of the solution vector have the order 10^{-16}.

In the third problem, we perform the simulation in the domain

$$\Omega = \{(x_1, x_2, x_3) \in \mathbb{R}^3 \mid -5 \le x_1 \le 5,\ 0 \le x_2 \le 0.2, \quad f(x_1, x_2) \le x_3 \le 1\}, \tag{39}$$

where $f(x_1, x_2)$ is given by (37) with $h_0 = 0.1$ and $a = 0.1$. Different grids have been used with the

characteristic dimensions of hexahedrons $\Delta x_1 \approx 0.25$, $\Delta x_2 \approx 0.025$, $\Delta x_3 \approx 0.25$. As in the above two cases, the L^1 errors are computed at the time $t = 5000$.

For the scheme with the AUSM U-splitting mass flux, we obtain the largest L^1 error for the pressure. Its value is 2×10^{-4}. The L^1 error for the velocity component v_2 in the direction perpendicular to the plane of motion has the order 10^{-12}. For other components of the velocity the L^1 error have the order smaller than 10^{-7}.

For the scheme with the density splitting the error for all variables is of the order of magnitude smaller than 10^{-4}, except of the longitudinal velocity components v_1, v_2. For these components the maximal errors which we have found were correspondingly 2.7×10^{-3} and 1.2×10^{-2}. The numerical error for v_2 is of the order of the grid size in the direction x_2. Our numerical experiments have shown that large errors for the velocity normal to the plane of motion are due to the Van Leer splitting in (28).

Notice that, for the static atmosphere, the results of test problems 1 and 3 can be compared. The comparison shows that no generation of spurious flows due to the presence of the orography occurs when the AUSM, U-splitting mass flux is applied. However, if the scheme with the density splitting is used, then, in the presence of the orography, the L^1 errors for the velocity components are larger. The maximal error is not better than $O(\Delta x_2)$.

4.2 *Potential flow*

Consider now the potential flow regime. If the orography is given by (37), then to compute this regime we have to satisfy the conditions: $h_0/a \sim O(1)$, $N a/U \ll 1$. Here the Brunt-Vaisala frequency N is defined by (36), U is the inflow velocity (used in (8), (12)). We perform the simulations in the domain

$$\Omega = \{(x_1, x_2, x_3) \in \mathbb{R}^3 \mid -0.125 \le x_1 \le 0.125, \quad 0 \le x_2 \le 0.025, f(x_1, x_2) \le x_3 \le 0.25\}, \quad (40)$$

where $f(x_1, x_2)$ is given by (37) with $h_0 = a = 5 \times 10^{-3}$. The thickness of the horizontal sponge layer is 0.125. Both vertical sponge layers have the thickness 0.06. On the boundaries of the domain (40), boundary conditions (7)–(9) are imposed. Initial conditions are given by (12), (13). In (8) and (13), the velocity U is equal to 0.0625.

The grid is presented in Fig. 1. The refinement is made near the lower boundary and over the mountain. The vertical dimension of hexahedrons Δx_3 has a value between 7.5×10^{-4} and 4×10^{-3}. The value of Δx_1 lies between 2.7×10^{-3} and 9×10^{-3}, $\Delta x_2 = 5 \times 10^{-3}$ for all cells.

The scheme with the density splitting is used. The isolines for the horizontal and vertical velocity are shown in Fig. 2a, 2b and that ones for the potential temperature are presented in Fig. 3. The results correspond to the time $t = 69.68$. The

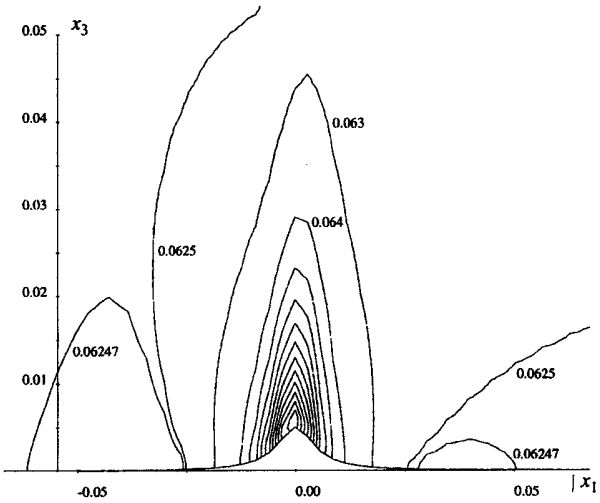

Fig. 2a. Potential flow case. Isolines of the horizontal velocity, with contour interval for the non-marked isolines equal to 0.001

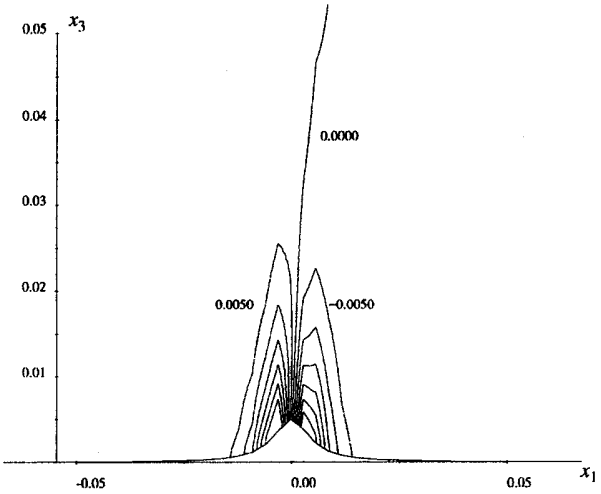

Fig. 2b. Potential flow case. Isolines of the vertical velocity with contour interval of 0.0005

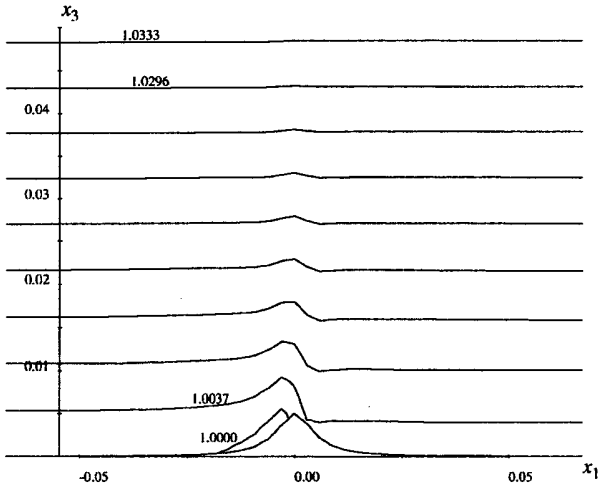

Fig. 3. Potential flow case. Isolines of the potential temperature with contour interval of 0.0037

quasisymmetrical structure of the potential flow is well realized, as can be seen in Fig. 2a, b. The structure of the potential temperature isolines shown in Fig. 3 confirms the absence of lee-waves. The computed values for the velocity v_2 turn out to be lower than 4×10^{-12} for all times. The structure of the isolines of the velocity components is similar to that one computed for this case by Pinty et al (1995). The structures for the potential temperature isolines are, however, different in a rather thick domain over the orography, as can be seen from comparison of Fig. 3 with Fig. 17 by Pinty et al (1995). We have already noted the fact that the numerical boundary conditions in our test problems correspond to the idealized thermally insulated mountain while that in the work by Pinty et al – to the mountain across which no potential temperature flux is transferred. In order to verify whether this fact is the reason of the difference, we have computed also this case with the thermal numerical condition as in Pinty et al (1995). But, again, we have obtained a structure very similar to that one shown in our Fig. 3. We assume that the difference can be explained by the difference in the discretization of the mountain surface. Our discretization is with linear slopes which are symmetric with respect to the symmetry plane of the agnesi profile while Pinty et al (1995) use the grid with the equally spaced vertical levels and with the horizontal levels which discretize the agnesi profile non-symmetrically as can be seen in Fig. 17. Note also, that the same results as shown in Figs. 2a, b and 3 were obtained in simulations in which we used the scheme with AUSM, U-splitting mass flux.

4.3 Linear hydrostatic regime

If the orography is given by (37), then we can compute the periodic waves in the linear hydrostatic regime by satisfying (see Pichler, 1997) the conditions: $h_0/a \ll 1$ and $N a/U \gg 1$ with N as in (36), and U the inflow velocity which we use in (8), (13).

To simulate this regime, we perform the simulations in the domain

$$\Omega = \{(x_1, x_2, x_3) \in \mathbb{R}^3 | -12.5 \leq x_1 \leq 12.5, \\ 0 \leq x_2 \leq 0.25, f(x_1, x_2) \leq x_3 \leq 1.2\}, \quad (41)$$

where $f(x_1, x_2)$ is given by (37) with $h_0 = 5 \times 10^{-5}$ and $a = 0.8$. The horizontal sponge layer has the thickness equal to 0.35. The vertical sponge layers have the thickness 1.6 in the case when the scheme with the AUSM, U-splitting mass flux is used. For the scheme with the density splitting, the thickness of both vertical sponge layers is equal to 3.2. The initial and boundary conditions are as in the previous case, however the inflow velocity U in (8), (13) is equal to 0.111.

The results presented in Fig. 4a, b have been simulated with the numerical scheme with the AUSM, U-splitting mass flux on the regular grid

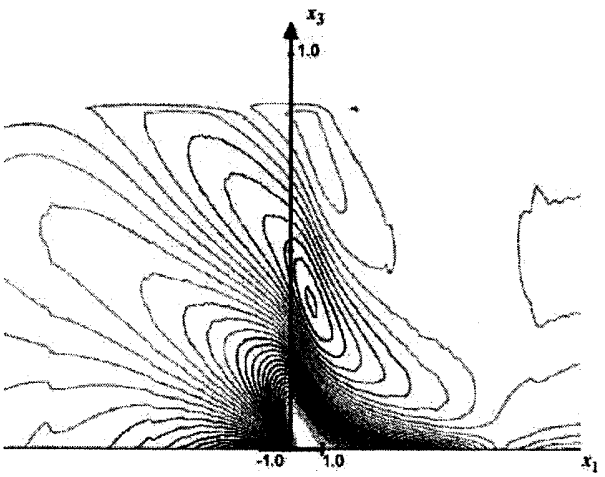

Fig. 4a. Structure of isolines of the horizontal velocity in a linear hydrostatic case, obtained at rescaled time $t = 56.82$ with the numerical scheme with the AUSM, U-splitting mass flux

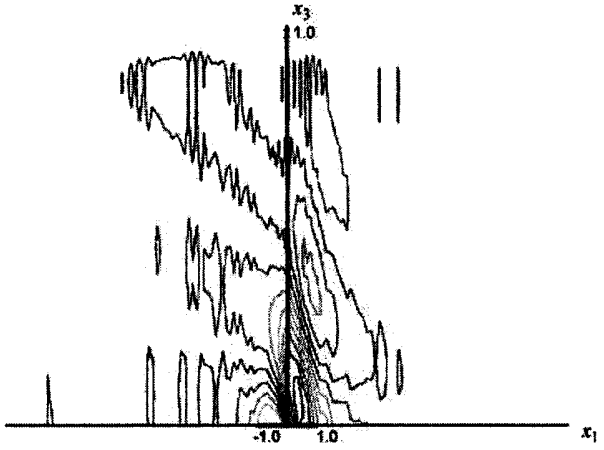

Fig. 4b. Structure of isolines of the vertical velocity in a linear hydrostatic case, obtained at the rescaled time $t = 56.82$ with the numerical scheme with the AUSM, U-splitting mass flux

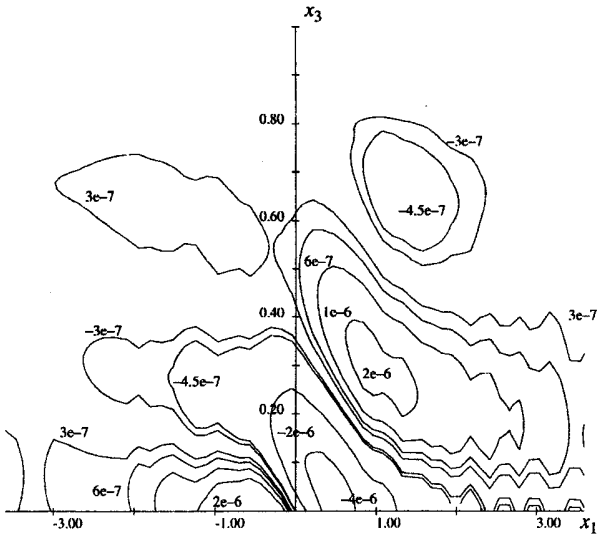

Fig. 5. Vertical velocity in a linear hydrostatic case at the rescaled time t = 69.35. Simulation is performed with the density splitting scheme

with the cell dimensions $0.156 \times 0.02 \times 0.125$. In Fig. 5, the scheme with the density splitting was used on the grid which, in comparison with the grid in Fig. 4a, b has a refinement on the bottom boundary. In Fig. 4a, the isolines of the horizontal velocity for the time $t = 56.82$ are presented. The figure shows that, at this time, the periodic structure of the gravity waves is already formed in the domain between the mountain and the sponge layer at the upper boundary. The structure of the horizontal velocity isolines obtained for the same time with the scheme with the density splitting is very similar to that one shown in Fig. 4a. Figure 4b shows the existence of a short wave numerical instability of the scheme with the AUSM, U-splitting mass flux. The results in Fig. 5 are presented for a later time ($t = 69.35$), a better resolution of the flow structure with the density splitting scheme can be seen here. The L^1 error for the velocity in direction normal to the plane of motion is equal to 4.6×10^{-5}. This error is considerably large compared with the error for the scheme with the AUSM, U-splitting mass flux, which has the order less than 10^{-10}.

4.4 Nonlinear non-hydrostatic regime

To compute the lee waves downstream the mountain (37) in the nonlinear non-hydrostatic regime, we have to choose the values of the mountain-parameters h_0, a and of the inflow velocity U in (8), (13) so that the condition $h_0/a \sim O(1)$, $N a/U \sim O(1)$ are satisfied.

We simulate this case in the following domain:

$$\Omega = \{(x_1, x_2, x_3) \in \mathbb{R}^3 | -1.25 \leq x_1 \leq 2.25, \quad 0 \leq x_2 \leq 0.25, f(x_1, x_2) \leq x_3 \leq 2\} \qquad (42)$$

for $f(x_1, x_2)$ defined by (37) with $h_0 = 0.045$, $a = 0.05$. The thickness of the horizontal sponge layer is equal to 1. For the left vertical sponge layer the thickness is equal to 0.25, and for the right one – to 0.25. Initial conditions are given by (12), (13) and boundary conditions – by (7)–(9). The inflow velocity U in (8), (13) is equal to 0.046.

The results obtained at the rescaled time $t = 44.45$ are shown in Figs. 6a, b, 7, and 8. The steady state is not yet reached. No essential difference between the results obtained with schemes (15)–(24) and (15)–(19), (21)–(23), (26)–(28), (30)–(33) have been found in this case. The computed L^1 errors for the component v_2 of the velocity vector have the order of magnitudes 10^{-5}, 10^{-12} for the schemes with the density splitting and with the AUSM, U-splitting mass flux, respectively. The results are presented in these figures for the numerical scheme with the density splitting on the grid refined near the bottom boundary and above the mountain, with the following characteristic dimensions: $\Delta x_1 \in (0.006, 0.017)$, $\Delta x_2 = 0.025$, and $\Delta x_3 \in (0.0035, 0.01)$.

In Fig. 6a, b, the structure of isolines is shown for the velocity components. The quasi-periodical

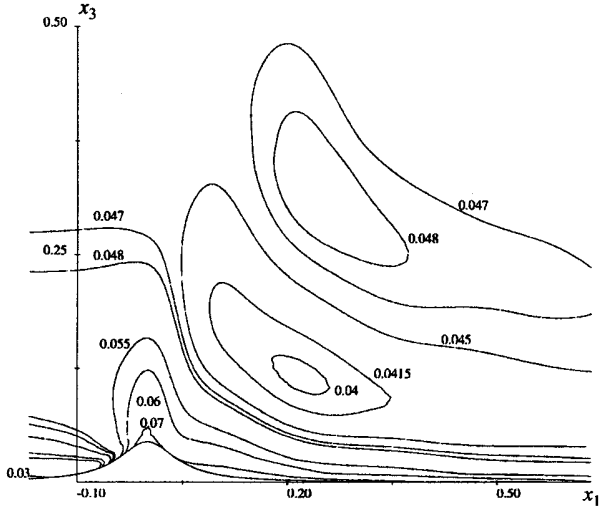

Fig. 6a. Horizontal velocity in a nonlinear non-hydrostatic lee wave test case at rescaled time $t = 44.45$. Numerical scheme is the density splitting scheme

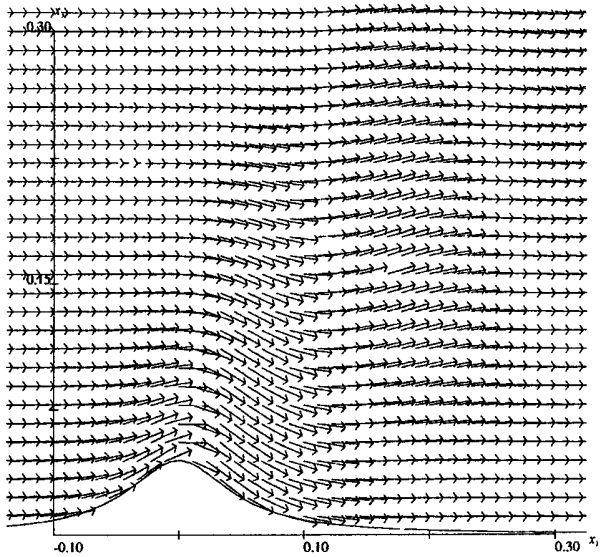

Fig. 7. Velocity field in a nonlinear non-hydrostatic lee wave test case at rescaled time $t = 44.45$. Numerical scheme is the density splitting scheme

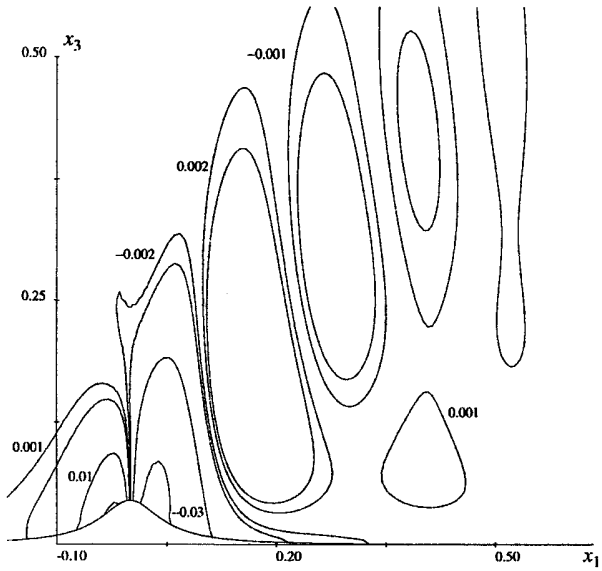

Fig. 6b. Vertical velocity in a nonlinear non-hydrostatic lee wave test case at rescaled time $t = 44.45$. Numerical scheme is the density splitting scheme

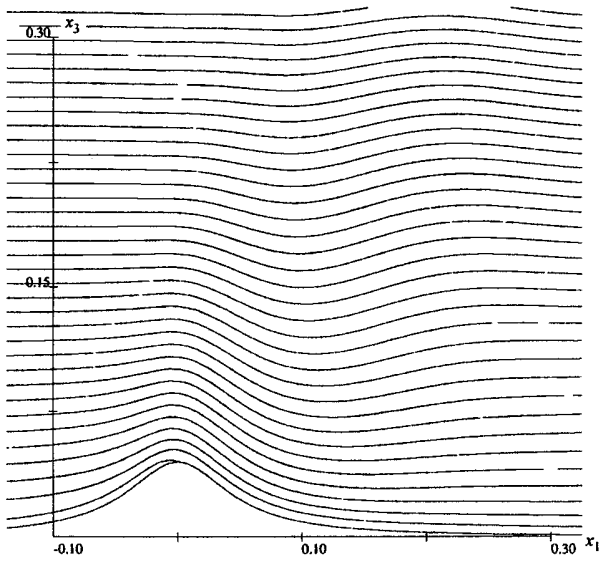

Fig. 8. Potential temperature in a nonlinear non-hydrostatic lee wave test case at rescaled time $t = 44.45$. Numerical scheme is the density splitting scheme

structure of lee waves is well reproduced. The flow accelerates down the mountain as in analogous test by Bonaventura (2000). Also, the structure of the velocity vectors near the mountain, shown in Fig. 7, is well resolved. The structure of the isolines of the potential temperature in Fig. 8 confirms existence of the lee waves.

5. Conclusion

In this paper, we have developed a finite volume scheme on unstructured hexahedral grids in 3D for the simulation of gravity waves arising around orographies. In our test problems we consider idealized orographies with a simple shape,

for approximation of which we use meshes of "finite-difference" type (structured grids). One example is shown in Fig. 1 where a vertical section of the mesh is presented. For the test problems, the hexahedral cells could be numbered with the help of a set i, j, k of integers i, j and k. But in our numerical code the grid cells are numbered individually, and, therefore, arbitrary unstructured grids can be considered. The use of unstructured grids can provide a better representation of complicated 3D-orographies by piecewise linear functions.

Two different discretizations have been suggested: the scheme with the AUSM, U-splitting mass flux given by (15)–(24) and the scheme with the density splitting defined by (15)–(19), (21)–(23), (26)–(28), (30)–(33). They have been tested for plane-parallel 3D atmospheric gravity waves. Good agreement of flow structures with that ones in the literature have been shown.

The scheme with the AUSM, U-splitting mass flux is similar in form to the AUSM schemes (see Liou, 1993; Liou and Wada, 1997). The difference is that we use the U-splitting only for the mass flux (20), but for all other components of the flux (16) we perform the splitting with the mass flux itself. The advantage of this scheme is that it produces no essential numerical errors in the direction perpendicular to the plane of motion. Its disadvantage is the existence of short acoustic waves revealed in the linear hydrostatic case.

In the scheme with the density splitting, we decompose the mass flux into two parts. One of them contains only the hydrostatic density $(\rho^0 v)_{ij}$ and is discretized by the AUSM, U-splitting. For the discretization of the mass flux $[(\rho - \rho^0)v]_{ij}$, we use the Van Leer's form of the splitting. In this scheme, the discretization of the normal momentum flux is also based on the decomposition of the density into two parts: ρ^0 and $\rho - \rho^0$. Calculated examples demonstrate the absence of the short acoustic waves. However, in the linear hydrostatic test problem, numerical errors for the velocity normal to the plane of motion are considerably large (see Sect. 4.3). The development of a higher-order discretization is therefore necessary to improve the resolution.

For the code we have used a data structure such that our tools for higher-order discretization, dynamic local mesh refinement and parallelization, including dynamic load balancing can be used very easily.

References

Adcroft A, Hill C, Marschall J (1997) Representation of topography by shaved cells in a height coordinate ocean model. Mon Wea Rev 125: 2293–2312

Bonaventura L (2000) A semi-implicit semi-Lagrangian scheme using the height coordinate for a nonhydrostatic and fully elastic model of atmospheric flows. J Comp Phys 158: 186–213

Egelja A, Kröner D, Schwörer R, Lanson N, Mancip M, Vila JP (1998) Combined finite volume and smoothed particle method. Preprint, Freiburg University. Freiburg 19: 25

Klemp JB, Lilly DK (1978) Numerical simulation of hydrostatic mountain waves. J Atmos Sci 35: 78–107

Kröner D (1996) Numerical schemes for conservation laws. Chichester Stuttgart: Wiley and Teubner, 508 pp

Küther M (2001) Error estimates for numerical approximations to scalar conservation laws. Doctoral Thesis, Freiburg University. Freiburg, 128 pp

Liou M-S (1993) On a new class of flux splittings. Lecture Notes in Phys 414: 115–119

Liou M-S, Steffen ChJ (1993) A new flux splitting scheme. J Comp Phys 107: 23–39

Oliger J, Sundström A (1978) Theoretical and practical aspects of some initial boundary value problems in fluid dynamics. SIAM J Appl Math 35: 419–447

Pichler H (1997) Dynamik der Atmosphäre. Heidelberg: Spektrum Akademischer Verlag, 572 pp

Pinty J-P, Benoit R, Richard E, Laprise R (1995) Simple tests of a semi-implicit semi-Lagrangian model on 2D mountain wave problems. Mon Wea Rev 112: 3042–3058

Schott P (2001) Dreidimensionale Strömungssimulation in der Wettervorhersage. Diploma Thesis, Freiburg University, Freiburg, 113 pp

Van Leer B (1991) Flux-vector splitting for the 1990s, CP-3078, NASA, Cleveland, OH, 203–214

Wada Y, Liou M-S (1997) An accurate and robust flux splitting scheme for shock and contact discontinuities. SIAM J Sci Comp 18: 633–657

Authors' address: L. Klassen, D. Kröner and Ph. Schott, Institute for Applied Mathematics, University of Freiburg, Hermann-Herder-Straße 10, D-79104 Freiburg, Germany (E-mail: dietmar@mathematik.uni-freiburg.de)